International Journal of Automotive Technology, Vol. 18, No. 1, pp. 165–177 (2017)
DOI 10.1007/s12239–017–0017–5

pISSN 1229–9138/ eISSN 1976–3832

DESIGN AND DEVELOPMENT OF AUTOMOTIVE BLIND SPOT DETECTION RADAR SYSTEM BASED ON ROI PRE-PROCESSING SCHEME

E. HYUN, Y. S. JIN and J. H. LEE*

ART (Advanced Radar Technology) Lab., DGIST Convergence Research Institute, DGIST,
333 Techno Jingang-daero, Hyeongpung-myeon, Dalseong-gun, Daegu 42988, Korea

(Received 13 April 2015; Revised 8 April 2016; Accepted 28 June 2016)

ABSTRACT–In the conventional 2D-FFT based target detection method, all range-Doppler cells are computed by FFT (Fast Fourier Transform) and scanned by CA-CFAR (Cell-Averaging Constant False Alarm Rate) detection. This results in high computational complexity and long processing time. In this paper, we developed an automotive 24 GHz BSD (Blind Spot Detection) FMCW (Frequency Modulated Continuous Wave) radar with a low complexity target detection architecture based on a ROI (Region Of Interest) pre-processing scheme. In the real BSD zone, because the number of cars to be detected is limited, the designed method only extracts their velocities corresponding to the range ROIs in which real targets exist. Moreover, the presence probability of vehicles with the same range-bin but different velocities is very low. Thus, in the designed method, some Doppler ROIs cells with a high magnitude are only applied for CA-CFAR detection. This architecture can dramatically reduce the amount of data to be processed compared to that of the conventional 2D FFT based method, resulting in enhanced processing time. We developed a 24 GHz FMCW radar system composed a transceiver, antennas, and signal processing module. The designed algorithm was implemented in a tiny micro-processor of the signal processing module. By implementing our proposed algorithm in the developed 24 GHz FMCW radar system in an anechoic chamber and a real road, we verified that the range and velocity of a car occupying the BSD zone were detected. Compared to that of the conventional method, the reduction ratio of the total processing time was measured to be 52.4 %.

KEY WORDS : Automotive radar, Blind spot detection radar, BSD radar, FMCW radar, Low complexity

1. INTRODUCTION

These days, driver-assistance systems have become one of the most important key technologies in intelligent transportation systems for decreasing the number of accidents (Lin *et al*., 2012). Vehicle accidents on the highway are very dangerous, because most cars are driving at a high speed and short range interval. On the highway, when the current lane is jammed, the driver usually prefers to change from the current lane into another one that appears to be empty, even though they are traveling at the same car speed (Lin *et al*., 2012). In that case, when the target lane is not empty, a fatal traffic accident occurs. This is because the vehicle's two side mirrors cannot help the driver observing the exact situation of the adjacent lanes due to limitations in the viewing angle (Lin *et al*., 2012). On highways with vehicles travelling at high speeds, a vehicle collision can give rise to very serious and dangerous situations with risk of successive crashes. Meanwhile, in urban area, drivers try to change the lanes and make turns many times while driving.

In both cases, driving without awareness of vehicles in the blind spot zone can cause vehicle accidents and injuries, as well as consequent traffic congestion.

To avoid collision accidents, some vehicles have deployed BSD (Blind Spot Detection) systems. The BSD system helps driver awareness of approaching vehicles in blind spot zones.

Recently, for monitoring blind spot zones, two main technologies based BSD systems have been released: radar and camera sensors either on the wing mirrors or at the rear of the vehicle (Fernández *et al*., 2013).

A typical example of a camera based BSD system is Volvo's Blind Spot Information System.

Compared to a radar sensor, cameras are inexpensive, but very sensitive under bad weather conditions such as rain, snow, heavy fog, and so on. To overcome this limitation, image processing can be carried out in various ways such as optical flow analysis or pattern recognition (O'Malley *et al*., 2010).

Good examples of radar based BSD systems are Audi Side Assist, Mercedes-Benz's Active Blind Spot Assist, and Infiniti's Blind Spot Warning. In particular, the use of radar based BSD systems has also increased for other rear collision avoidance applications such as LCA (Lane Change Assistance) systems, RCTA (Rear Cross Traffic Alert)

**Corresponding author.* e-mail: jhlee@dgist.ac.kr

systems, and PAS (Parking Assistance Systems). To support various functions with one radar sensor, in most vehicles, the radar based BSD sensors are mounted inside the rear bumper of the vehicle (Forkenbrock *et al*., 2014).

Compared to the vision sensors, the radar sensor can guarantee system reliability, irrespective of the weather or road conditions. Moreover because the automotive radar sensor can provide the position and velocity of the target object, approaching vehicles in the blind spot zone are easily distinguished (Jeong *et al*., 2012).

In recent years, on chip radar transceivers with high-density have been released, providing compact design and cost effectiveness. Thus, in the future, the radar sensor will be important together with camera sensors for driver-assistance systems.

Generally, FMCW (Frequency Modulation Continuous Wave) radar has been used for automotive radar (Jeong *et al*., 2012). In FMCW radar, the frequency difference between the transmitted source and the received signal is used to detect the range and velocity. Since the bandwidth of a received beat signal can decrease to be less than a dozen MHz, regardless of the transmitted bandwidth, the hardware complexity of the signal processing part can be reduced compared to that of the pulse radar (Richards, 2005; Lee and Kim, 2010).

The FMCW modulation scheme is an effective method, but this method possesses ambiguities regarding the separation of the range and the velocity for multi-target situations (Shunji, 2004; Winkler, 2007). In order to resolve these ambiguities, a fast-ramp based FMCW radar has been proposed (Shunji, 2004; Winkler, 2007). In this method, by doing the FFT processing, every single ramp mainly extracts target range information. Next, the Doppler frequency is obtained through additional FFT processing of the discrete data in each range-bin over a PRI (Pulse Repetition Interval), where a 2D-map of the range and Doppler frequency spectrum is completed. Finally, in order to obtain the range and velocity of the target from the range-Doppler map, the CA-CFAR (Cell-Averaging Constant False Alarm Rate) detection is carried out in the Doppler direction for every range-bin (Winkler, 2007).

While 2D-FFT based processing using fast-ramps is an effective detection method for target ranges and velocities, the necessary computational effort is very high. Since all cells of the 2D range-Doppler map should be scanned, especially for CA-CFAR detection processing, the entire processing time can dramatically increase.

Automotive BSD radars should quickly provide drivers with reliable target information because the detection zone is very narrow. Therefore, the required signal processing time is extremely short. Moreover, in an automotive radar, since a low cost micro-processor for the signal processing module is required, the computational complexity of the target detection algorithm is more important.

Thus, in this paper, we designed a low complexity target detection architecture. We also developed a 24 GHz BSD FMCW radar system composed of a transceiver, antenna, and signal processing module. In the developed signal processing module, the tiny micro-processor was employed to implement the designed target detection architecture.

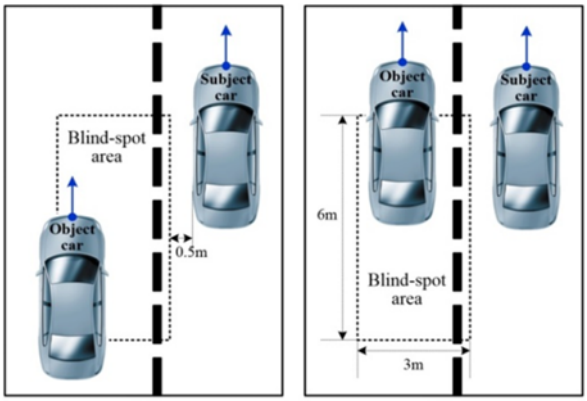

Figure 1. Blind spot warning requirements based on the requirement of ISO document.

In order to reduce the computational complexity, we first should consider the blind spot warning requirements described in the ISO (International Organization for Standardization) document (ISO, 2008). Figure 1 shows the blind spot warning scenarios.

The radar system of the subject car should determine whether the object vehicle is present in the blind spot area. In case of Figure 1 (a), the blind spot detection radar must give a warning to the driver because the object car is ahead of the lowest line of the BSD zone. In Figure 1 (b), the BSD warning may or may not be needed because the object vehicle is not entirely behind the most upper line of the BSD zone. Therefore, according to the position of the object occupying the blind spot zone, the BSD radar system installed on the subject vehicle must warn, may warn, or must not warn the driver (ISO, 2008).

Taking into consideration of the general vehicle size and coverage of the blind spot zone, we propose two reasonable and possible assumptions for the BSD application:

Every vehicle is not present in every range-bin.

The presence probability of multiple vehicles having different velocities in the same range-bin is very low.

Based on these assumptions, we designed detection architecture with two ROI (Region of Interest) pre-processing schemes in order to reduce the processing complexity based on the 2D-FFT algorithm.

First, we applied Doppler-processing and CA-CFAR detection to only the range of interest where the real target can exist. For that, after range-processing, we added the range ROI detection part to determine the range-bins where targets can exist. Compared to that of the conventional 2D FFT based method, in which all kind of processing part are used for all range-bins, the computational complexity can be reduced when the designed method is used.

Next, we added the Doppler ROI finding function before CA-CFAR detection. In the conventional architecture, the CFAR detector scans all cells of the 2D-map in order to determine whether each cell is the target or not. However, in the designed method, only Doppler ROI cells are applied for CFAR detection.

From a processing time point of view, compared to the conventional method, the designed method can decrease the required time because the number of scans is reduced. Since the reduction of the total processing time will ultimately enhance the potential of crash prevention in the blind spot zone, the proposed scheme is very useful for BSD systems.

In Section 2, the conventional 2D-FFT based detection method is presented. Section 3 describes the designed target detection scheme for BSD radar application. Section 4 presents the consideration of processing complexity. In Section 5, the results of the development and implementation are given. Section 6 presents experimental results in an anechoic chamber and a real road. The conclusions from our study and the directions for future work are presented in Section 7.

2. CONVENTIONAL 2D-FFT BASED DETECTION OVERVIEW

According to the FMCW radar with a fast-ramp (Shunji, 2004), the frequency-time domain plot of the transmit waveform is shown in Figure 2 (a). Here, B is the bandwidth, and T is the pulse repetition period. The 2D-FFT based signal processing scheme can be divided into three steps, as shown in Figure 2 (b): The range-processing part, Doppler-processing part, and CA-CFAR detection part.

The whole processing procedure is as follows:

① Range processing part

- The received signal is digitalized by ADC (Analog Digital Converter) with a sampling frequency of f_s.
- The sample $\{SR(s, l), s = 1 \sim S, l = 1 \sim L\}$ is transformed by the N-point FFT into the frequency domain within each ramp in order to generate the frequency spectrum for the target range. Here, S is the sample size in one ramp and L is the number of ramps in one frame time.
- All extracted range spectra $\{RR(n, l), n = 1 \sim N, l = 1 \sim L\}$ are also stored. Here, N is the number of range-bins in each ramp.

② Doppler-processing part

- The Doppler spectrum $\{RD(n, m), n = 1 \sim N, m = 1 \sim M\}$ is estimated by M-point FFT processing inside a single range-bin over a sequence of adjacent ramps and is saved.

③ CA-CFAR detection

- Generally, in the 2D range-Doppler map, the CFAR detection can be done directly in the Doppler spectrum. This is because the number of targets in one Doppler spectrum is low in practical cases (Winkler, 2007).

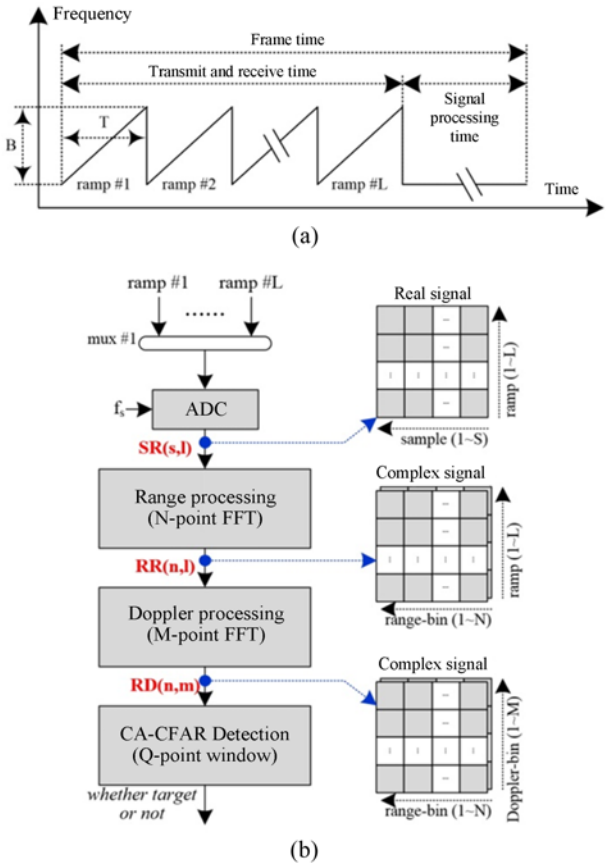

Figure 2. Concept of a fast-ramp based FMCW radar: (a) Frequency-time domain plot of the transmit waveform; (b) Target detection procedure.

Thus, the Doppler magnitude spectra of the n^{th} range-bin are selected as test cells such as $(RD(n, 1))^2 \sim (RD(n, M))^2$.

- Each test cell is sequentially scanned with the Q-point sliding window. At the same time, the corresponding threshold is calculated by averaging and scaling the reference cells. Here, the reference cells are composed of cells on the right and left sides of the test cell in one window.
- If the test cell's magnitude is greater than a certain threshold, the test cell can be determined as the target.
- The procedure is performed until all test cells in one Doppler spectrum are scanned. The procedure is repeated until the data of all range-bins are selected.

3. DESIGN TARGET DETECTION SCHEME FOR BSD RADAR APPLICATIONS

The conventional 2D-FFT based target detection method should be used to generate the entire 2D range-Doppler map. Moreover, in CA-CFAR processing, all test cells of the 2D-map should be scanned. This results in high computational complexity.

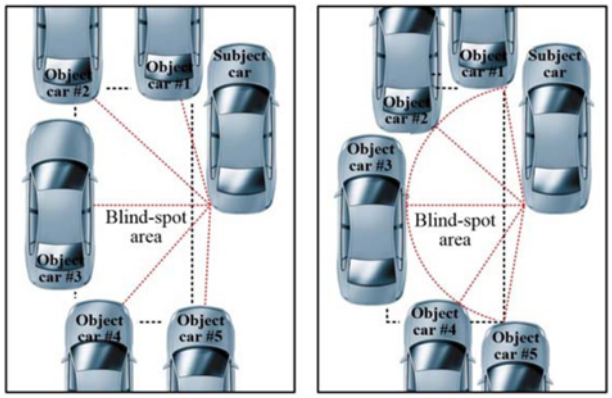

Figure 3. Example of multiple vehicles occupying blind-spot zone at the same time.

Thus, in this paper, we designed a low complexity target detection architecture based on the ROI pre-processing for blind spot detection radar.

In order to do that, after considering the BSD warning requirements together with the narrow blind-spot zone size and general vehicle size, we propose two reasonable and possible assumptions as follows:

First, every target is not present in every range-bin. That is, in the BSD zone, the number of cars to be detected is limited.

Second, the presence probability of multiple vehicles with different velocities in the same range-bin is very low.

In order to explain the proposed assumptions for the BSD radar application, we illustrate two examples based on the BSD zone and the general car size.

Figure 3 (a) shows that the maximum number of vehicles to be detected in different range-bins is about 5. In that case, since multiple scatterings can be reflected from one car, the detected range-bins can be more than the number of real cars. Next, Figure 3 (b) shows the driving cars to be detected in the same distance, and their maximum number is also 5.

In reality, however, we expect that the number of vehicles present in the blind-spot zone is less than 5, because there is an actual driving interval between moving cars.

These two reasonable assumptions, as mentioned above so far, are the reason for the ideas created to reduce the target detection processing complexity for BSD radar system. Thus, we designed the blind-spot detection processing scheme, as shown in Figure 4.

Compared to the general 2D-FFT based detection method, two ROI pre-processing blocks are added: The range ROI detection part before the Doppler processing part and the Doppler ROI finding function before CA-CFAR processing.

The steps for the designed target detection process are as follows:

① Range processing part

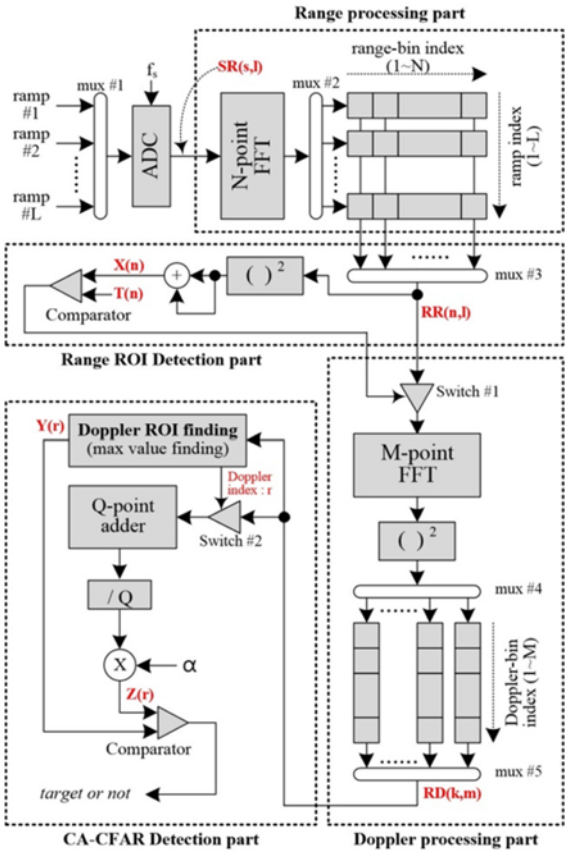

Figure 4. Designed target detection processing architecture using ROI pre-processing scheme.

- Like the conventional method, the N-point FFT processor transforms the received signal $SR(s, l)$ into the frequency spectrum $RR(n, l)$. Here, the 2D map dimension is the range-bin index and ramp index.

② Range ROI detection part

- First, in order to generate the range-profile expressed as the frequency magnitude spectrum, the complex absolute computations are carried out for all ramps.
- Second, for non-coherent summations, an accumulator integrates the range-profile for every L ramp. This is to improve the SNR (Signal to Noise Ratio) relative to that of the single ramp (Bassem and Atef, 2004).
- Finally, when comparing the integrated range-profile $X(n)$ and the threshold $T(n)$, each range-bin with a high target presence possibility was determined. For that, $T(n)$ was set as the minimum power value.
- Figure 5 (a) shows the procedure and results of the range ROI detection part in detail. The red circles marked on a 2D memory block containing $RR(n, l)$ indicates the selected range ROI cells.

③ Doppler-processing part

- Only the selected $RR(n, l)$ is fed into the Doppler processing part in order to activate switch #1.
- The processing results are saved as $RD(k, m)$, where $k \in \{1 \sim K\}$ is the ROI index, such as the data map

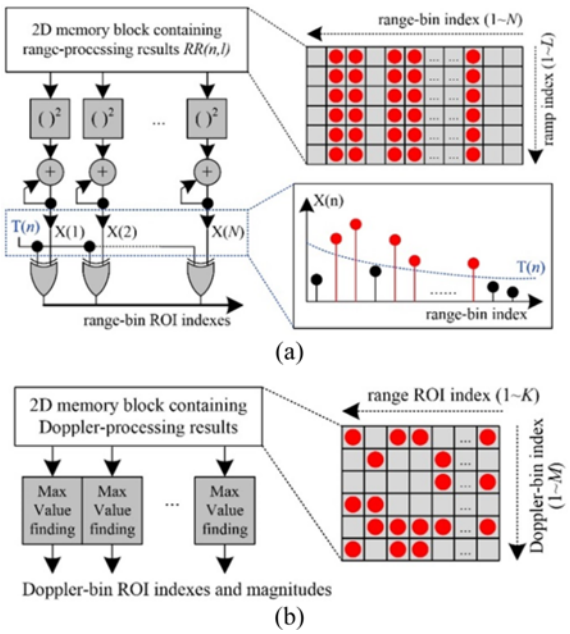

Figure 5. Two ROI pre-processing architectures, where, red circle marks indicate the found range or Doppler ROI cells: (a) Results of the range ROI detection part; (b) Results of the Doppler ROI finding.

described in Figure 5 (b). Here, the vertical direction represents the Doppler-bin index and the horizontal direction represents the range ROI index.

④ CA-CFAR detection part

- First, in the Doppler ROI finding block, from the Doppler-spectrum of a range-bin of kth ROI switched by mux #5, the Doppler ROI finding function selects test cells of interest with a high magnitude by using the max value finding processing. Here, $r \in \{1 \sim R\}$ represents the selected Doppler ROI cells with the magnitude $Y(r) = RD(k, r)$.
- Figure 5 (b) shows the results of the Doppler ROI finding in detail. Here, for example, three cells with a high magnitude per one range are displayed as red circle marks.
- Then, for test cells $Y(r)$, the corresponding reference cells are also selected through switch #2. The threshold is calculated using an averaging function and multiplier. Then, it is determined whether the test cell $Y(r)$ is a target or not.
- The procedure is repeated until the Doppler-spectra of all range ROIs have been selected by mux #5.

In the designed target detection architecture, the additional Range ROI detection part and the Doppler ROI finding in the CA-CFAR detection part can dramatically reduce the whole processing complexity. The reason is described in detail as follows:

- While the Doppler-FFT and CA-CFAR detection are performed until all range-bins are scanned in the conventional 2D-FFT method, in the designed method, the Doppler-processing and CA-CFAR detection are only performed for the range-bins selected in the range ROI part.
- While the CA-CFAR detection is repeated until all 2D range-Doppler maps are scanned in the conventional detection method, the CA-CFAR detection of the designed method is only carried out for the Doppler-bins that have test cells selected from Doppler ROI finding.

In summary, the proposed target detection scheme can reduce the total processing time using two ROI pre-processing steps. Thus, the proposed method ultimately offers a sufficient time margin to deal with crash prevention in the blind spot zone. Moreover, it can be useful for vehicle safety systems at competitive prices.

4. CONSIDERATION OF PROCESSING COMPLEXITY

In order to implement signal processing for a BSD radar and consider the computational complexity, we employed the Texas Instruments TMS320 processor, which is a tiny processor with a 32 bit floating point core.

For the used C28x core, TI has released a collection of highly optimized application functions in a library (Texas Instruments, 2012). Among the functions of the library, we used the following functions: complex FFT, computation of the absolute value of a complex vector, the mean of vectors, and finding from the index on the maximum value of a real array. The cycle counts of these functions are presented in Tables 1 and 2, where D is the data length.

Table 1. Cycle counts of FFT.

FFT point (D)	32	64	128	256	512	1024
Cycle count : *C_FFT (D)*	1,121	2,231	5,029	11,023	24,249	53,219

Table 2. Cycle counts of other libraries.

Function	ABS	Mean	Find max value
Library name	abs_SP_CV_2	mean_SP_CV_2	Maxidx_SP_RV_2
Cycle count	*C_ABS (D) = 18*D + 22*	*C_MEAN (D) = 2*D + 34*	*C_MAX (D) = 2*D + 21*

Table 3. Processing time complexity comparison.

	Conventional architecture	Designed architecture
Range-FFT	*C_FFT (N) * L*	*C_FFT (N) * L*
ROI selection	Not need	*[C_ABS (L) + C_MEAN (L)] * N*
Doppler-FFT	*[C_FFT (M) + C_ABS (M)] * N*	*[C_FFT (M) + C_ABS (M)] * K*
CA-CFAR detection	*C_MEAN (Q) * M * N*	*[C_MAX (M) + C_MEAN (Q)] * K * R*

Based on these cycle counts, Table 3 summarizes the target detection processing complexity of the conventional method, which is composed of a range-processing part, a Doppler-processing part, and a CA-CFAR detection part. Here, L is the number of ramps, N is the range-bin length, M is the number of Doppler-bins, and Q is the window size. Table 3 also describes the designed target detection scheme with an additional range ROI detection part and Doppler ROI finding. Here, K is the number of range ROIs, and R is the number of Doppler ROIs.

While all parts of the conventional method are carried out until all 2D range-Doppler cells are scanned, the Doppler-processing and CA-CFAR detection parts of the designed architecture are processed for only K range ROIs. Moreover, the conventional CA-CFAR detector should scan all M by N cells, whereas the CA-CFAR processing of the designed method treats only K by R ROI cells selected through finding the maximum values.

Based on the results shown in Table 3, we simulated the total processing cycle counts for the conventional and designed target detection architectures with results shown in Figures 6 and 7. Here, the x-axis is the range-bin size $N \in \{32, 64, 128\}$ and the y-axis indicates the normalized cycles count. Moreover, the Doppler-bin sizes $M \in \{32, 128\}$ are applied, respectively.

In order to compare the cycle counts of the designed architecture, we considered four cases together including the conventional architecture shown in Table 4. That is, various range ROI sizes (K) were considered in the simulation. In that case, we selected the number of Doppler ROI (R) as 5, which is based on the analysis results in Figure 3.

As can be seen in the results of Figures 6 and 7, even though the range ROI detection part is not applied but the Doppler ROI finding in CA-CFAR is only applied (case (b)), the computational complexity is dramatically reduced. Moreover, from the results of cases (c) ~ (d), including both ROI pre-processing schemes, it is proved that the cycle counts of the total processing decrease when the number of range ROIs is smaller.

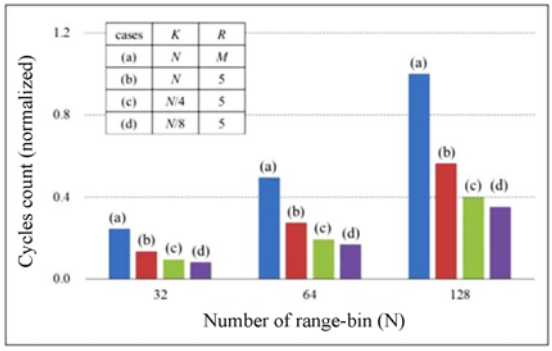

Figure 6. Total processing cycle count for the typical method and the proposed methods with $M = 128$.

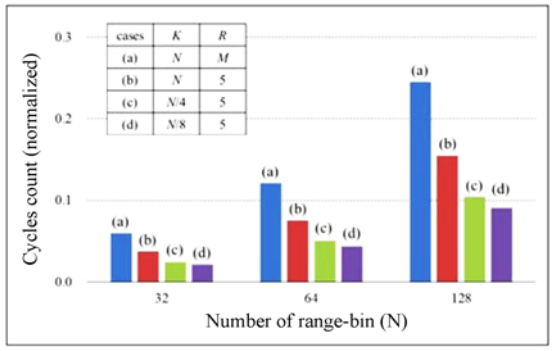

Figure 7. Total processing cycle count for the typical method and the proposed methods with $M = 32$.

Table 4. Various simulation cases for comparisons of computational complexity.

Case	Range ROI size (K)	Doppler ROI size (R)	Description
(a)	N	M	Range ROI detection and Doppler ROI finding are not applied.
(b)	N	5	Range ROI detection part is added, but Doppler ROI is not applied.
(c)	N/4	5	Both ROI pre-processing schemes are applied.
(d)	N/8	5	Both ROI pre-processing schemes are applied.

In summary, we can reduce the computational load burden considerably by appropriately selecting the number of ROIs to be analyzed before Doppler-FFT and CA-CFAR processing.

5. DEVELOPMENT AND IMPLEMENTATION OF BSD RADAR SYSTEM

We developed a 24 GHz BSD radar to verify the designed target detection architecture. Generally, the 24 GHz radar has been used for short range and wide angle detection such as BSD, LCA (Lange Change Assist), and RCW (Rear Crash Warning) systems (Jeong *et al*., 2012). The developed 24 GHz BSD radar system specifications and signal processing parameters are presented in Table 5.

In order to support the radar specifications described in Table 5, a block diagram and photo of the developed 24 GHz FMCW BSD radar system are presented in Figures 8 and 9.

First, we developed a 24 GHz radar transceiver. The single transmitter consists of a VCO (Voltage Controlled Oscillator), a frequency synthesizer, and an oscillator in order to generate a FMCW source, which has 200 MHz bandwidth over the range of 24.05 GHz ~ 24.25 GHz with 10 dBm output power, as shown in Figure 10. The developed receiver is comprised of one RF part and two IF channels: one LNA (Low Noise Amplifier), one I/Q mixer, two HPFs (High Pass Filters), and two LPFs (Low Pass Filters). The received RF signal is down-converted to two IF signals in an I/Q mixer.

Next, we developed 24 GHz transmitting and receiving antennas. The transmitting antenna is composed of an array in order to shape the beam-pattern so as to effectively cover the BSD zone. The measured radiation pattern of the antenna with horizontal polarization is shown in Figure 11.

Table 5. System specifications for the developed BSD radar.

Specification	Value
Center frequency	24 GHz
Bandwidth (B)	200 MHz
Pulse repetition time (T)	80 us
Ramp size in one frame (L)	64 ramp
ADC sampling rate (f_s)	500 KHz
Sample size in a single ramp (S)	40 sample
Range-FFT point (N)	64 point
Doppler-FFT point (M)	64 point

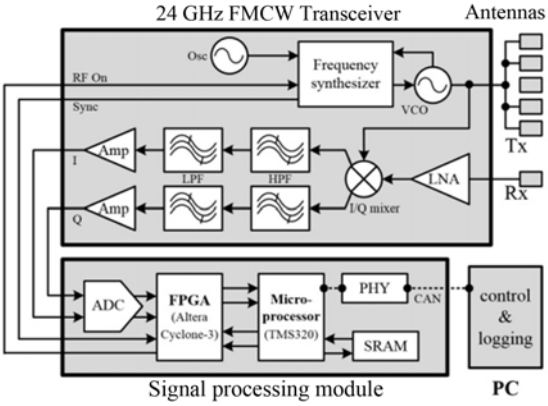

Figure 8. Block diagram of the 24 GHz FMCW BSD radar system composed of signal processing module, transceiver, and antennas.

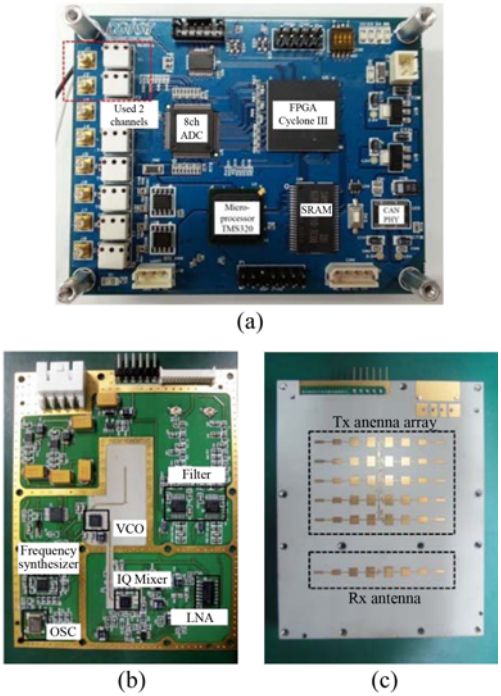

Figure 9. Photos of the 24 GHz FMCW radar system: (a) Signal processing module; (b) Transceiver; (c) Antennas.

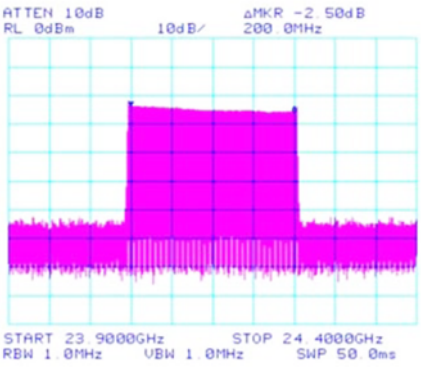

Figure 10. Measured transmitted signal with the frequency 24.05 GHz ~ 24.25 GHz.

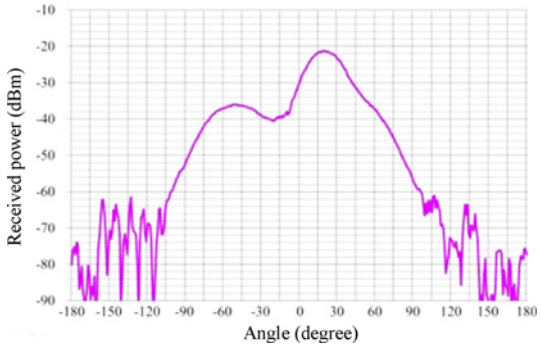

Figure 11. Measured radiation pattern of the 24 GHz transmitting antenna.

The receiving antenna has a symmetric fan shaped beam pattern with a 3 dB beam-width of 32°.

For the signal processing module, an Analog Device AD9252 ADC, Altera Cyclone-III FPGA, and a Texas Instruments TMS320 micro-processor were used. The TMS320 is a tiny micro-processor with a 32 bit floating point core, in which the blind-spot detection algorithm was implemented. The FPGA is only a bridge controller for the interface between the micro-processor and the external ADC. The target detection results are transferred into a PC via a CAN (Controller Area Network) interface.

We measured the total processing time for the target detection functions implemented in TMS320, with results as shown in Table 6. In this case, the processing clock of the micro-processor is 100 MHz.

In order to compare the signal processing time of the developed radar, we also considered four cases. The description of each case is already mentioned in Table 4. Here, the $R = M$ of case (a) and $K = N$ of cases (a) and (b) mean the Doppler ROI finding function and the range ROI detection part are not employed, respectively. In contrast, in cases (c) and (d), two ROI pre-processing procedures are applied.

In the results, the consumed time of case (b) dropped to 17.01 ms compared to the general detection architecture (case (a)) with a processing time of 28.22 ms. Moreover, in cases (c) and (d), the reductions in the computational complexity were obtained as 52.37 % and 56.38 %, respectively.

Table 6. Processing time for the micro-processor (processing clock 100 MHz).

Case	(a)	(b)	(c)	(d)
Range ROI sizes (K)	N (= 64)	N (= 64)	$N/4$ (= 16)	$N/8$ (= 8)
Doppler ROI sizes (R)	M (= 64)	5	5	5
Processing time (ms)	28.22	17.01	13.44	12.31

For the real driving field test, we used the algorithm implementation based on case (c). The details are described in Section 6.2.

6. EXPERMENTAL RESULTS

6.1. Measurement in an Anechoic Chamber

To verify the developed radar system, we prepared a measurement set-up in an anechoic chamber located at DGIST (Daegu-Gyeongbuk Institute of Science & Technology) in Korea, as shown in Figure 12. The developed radar system was mounted on the positioner. Here, in order to analyze the experimental radar data of each algorithm step, the JTAG (Joint Test Action Group) cable was linked between a PC and the signal processing module.

We carried out three experiments in the chamber environment. First, we measured the target detection according to the vertical installation position for the radar system, shown in Figure 12 (a). Here, a 30 cm by 30 cm rectangular reflector was used, as seen in the left photo of Figure 13. The radar system is located at 15 cm height, arranged the perpendicular to the target. We set this location as the reference position. We then measured the respective range profile by vertically raising the radar

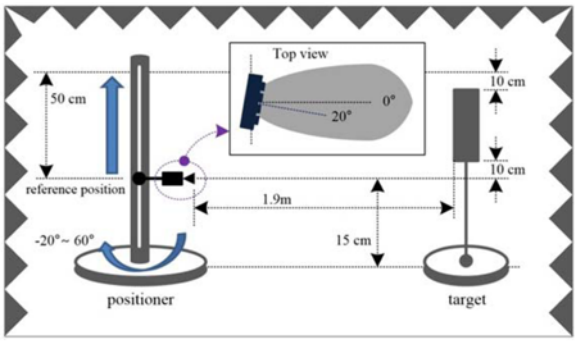

(a)

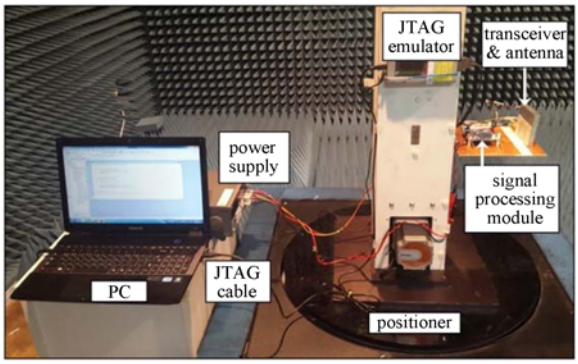

(b)

Figure 12. Measurement of the vertical radar installation position: (a) Set-up configuration in clean chamber room; (b) Photo of radar system mounted on positioner (lower).

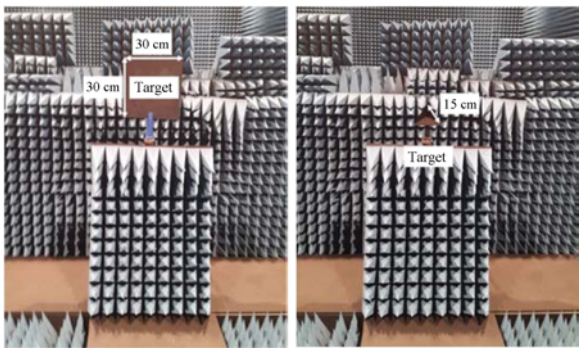

Figure 13. Photo of target for radar testing based on the installed vertical position (left) and the installed tilt angle (right).

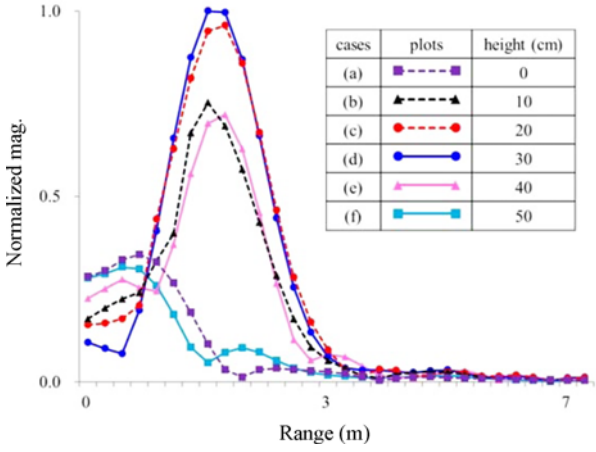

Figure 14. Measurement results for radar testing based on the installed vertical position.

system, from 0 cm (reference position) to 50 cm by 10 cm increments.

Figure 14 shows that the measured range profile spectra according to each installation height. Here, the x-axis is the range (in meters) and the y-axis is the normalized magnitude.

From the experimental results, the vertical installation positions with heights of 10 cm through 40 cm, except for only two cases (a and f), with heights of 0 cm and 50 cm, have good target detection. This means that the developed radar system has a vertical installation margin ranging up to approximately 30 cm.

Second, we measured the target detection according to the installation tilt angle of the developed radar system.

As seen in Figure 12 (a), we used the same experimental setup for measuring the effect of the installation angle on the target detection. On the other hand, a single reflector with a triangular pyramid was used, as presented in the right photo of Figure 13. The radar system was initially installed at a 20° tilt angle, as shown in Figure 11. We then measured the target detection of the radar system by

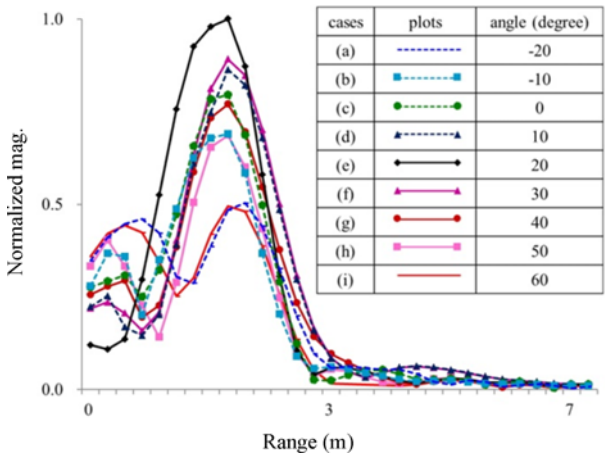

Figure 15. Measurement results for radar testing based on the installation angle.

varying the installation angle from – 20° to 60° with a 10° increment.

Figure 15 shows the measured range profile spectra according to each installation tilt angle. Here, the x-axis is the range (in meters) and the y-axis is the normalized magnitude. From the experimental results, the installation tilt angle with – 10° through 50°, except for only two cases (a and i) with tilt angles of – 20° and 60° have a good target detection. The peak in the range profile corresponds to at about a 20° installation tilt angle. This means that the developed radar system has a detectable field of view of up to approximately 60°.

Finally, to evaluate the detection performance of the developed radar system in a multi-target environment, we made experiments with three targets shown in Figure 16. Two stationary targets were placed at about 1.2 m and 2.7 m, respectively. Moreover, the single target was moving on rail between 2 m and 5.4 m with less than 4 km/h speed.

Figure 17 shows the measured range-velocity maps. Two stationary targets were seen at 1.17 m and 2.58 m, respectively. In addition, the moving target was also seen at 3.28 m with 4.38 km/h. Notably, at 5.39 m, this target stopped instantaneously with zero velocity because of the turning point to change the direction. Here, the x-axis is

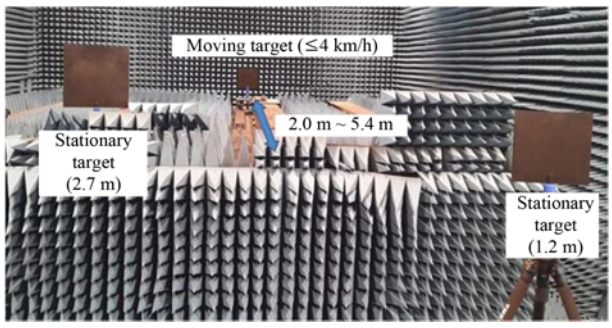

Figure 16. Measurement set-up for multi-target detection.

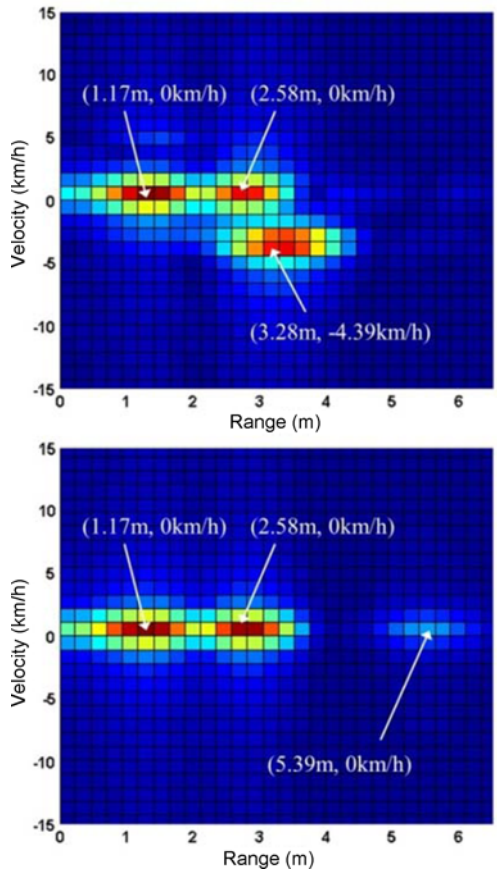

Figure 17. Measurement detection results for multi-target: A moving target is going away (upper) and a moving target stops at about 5.4 m (lower).

range (in meters), the y-axis is velocity (in km/h), and the color represents the normalized magnitude.

6.2. Real Driving Field Test

To verify the detection performance of the developed 24 GHz BSD radar on a real field, we carried out the detection of a target occupying the BSD zone. Figure 18 (upper) illustrates the concept of our measurement environment, where a real single car passed through the detection zone.

We conducted experiments with the developed radar installed at a fixed position because additional equipment was not available to mount the developed radar on a subject vehicle. Thus, we also considered only clear daytime to prevent dangerous situations. Here, the installation height from the ground and the installation tilt degree are 50 cm and 20°, respectively.

Figure 18 (lower) schematically illustrates the experimental set-up. To initiate the developed radar system and obtain the detection results, the PC was interconnected with the signal processing module via CAN. The camera was also used as a monitor system in the BSD zone.

Using the measurement setup for a real field test, we considered three scenarios.

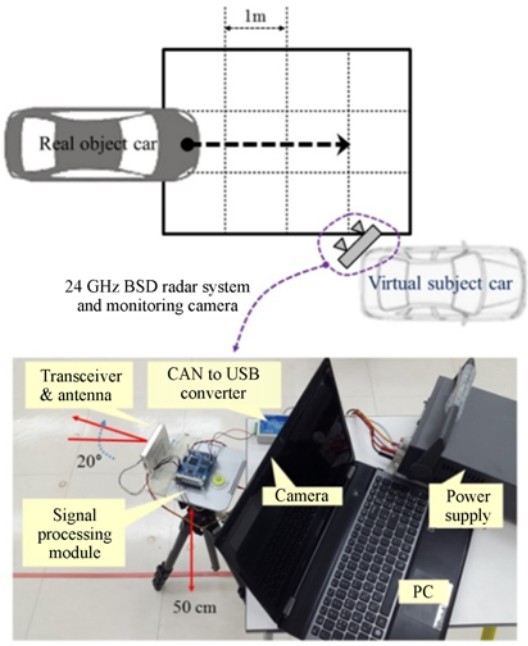

Figure 18. Example of the measurement environment for blind-spot detection radar: Top view of the experimental configuration (upper) and photo of set-up using the radar system mounted on a tripod (lower).

In the first scenario, to determine whether the developed radar meets the BSD spot warning requirements (see Figure 1), two cases were considered. That is, the object car was driving along the nearest line and the farthest line within a BSD zone with about 20 km/h on the open road located in DGIST. The captured camera images are shown in Figure 19.

Figure 20 shows the measured target detection results using the proposed detection scheme. As mentioned in Section 5, the range ROI (K) and Doppler ROI (R) are selected as 16 (= N/4) and 5. Here, the x-axis is the range (in meters) and the y-axis is the radial velocity (in km/h).

The measured range is the distance between the radar and the driving car. In addition, the measured radian velocity is the component of the object's velocity that points in the direction of the radius connecting the object and the radar. In the results of Figure 20, positive radial

Figure 19. Camera views of the first scenario on an open road: Driving car along the nearest line (left) and the farthest line (right).

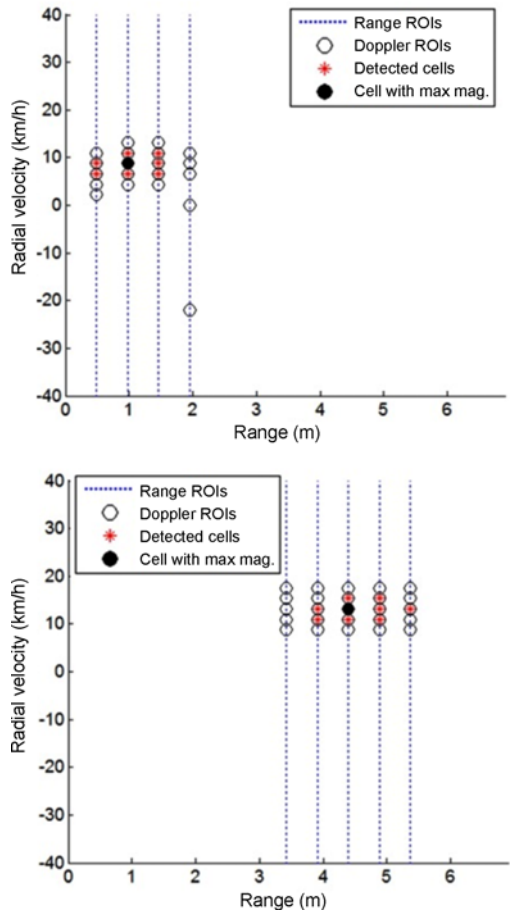

Figure 20. Measured target detection results on open road: the driving car along the nearest line (upper) and the farthest line (lower).

velocities indicate that the vehicle is approaching the radar. Negative values, meanwhile, mean that the vehicle is moving away from the radar.

The blue dotted lines indicate the range-bins selected during the range ROI detection step. In the experimental results, just 4 and 5 range-bins survive by thresholding. Black circles are velocity-bins selected in Doppler ROI finding, where 5 Doppler bins were determined per range ROI. The red star marks indicate the final detection results using CA-CFAR detection.

Even though only one car passes through the blind-spot zone, multiple scatterings exist in the range and velocity map. Among them, the strongest was displayed as a black solid circle indicating that the range and velocity in the nearest and the farthest are 0.98 m and 8.79 km/h and 4.39 m and 13.18 km/h, respectively.

In the second scenario, we considered three types of targets including a car, a bicycle, and a human on an urban road near DGIST, as seen in Figure 21. Here, several cars were parked at one side of the road. A car, a bicycle, and a pedestrian were approaching the developed radar system through BSD zone.

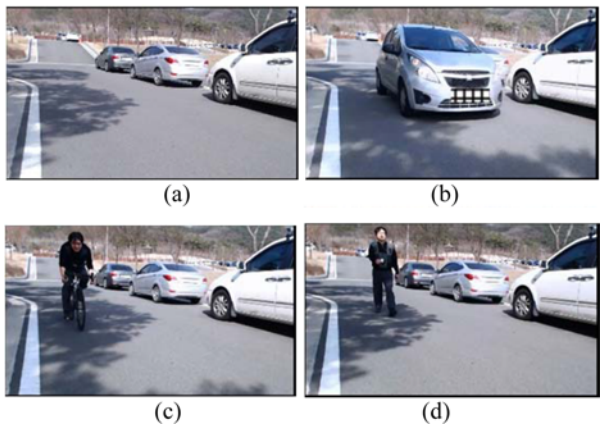

Figure 21. Camera views of the first scenario on urban road: (a) Just parked cars; (b) Moving car; (c) Moving bicycle; (d) One pedestrian.

Figure 22 shows the measured target detection results of the proposed method for various targets. Here, the x-axis is the range (in meters) and the y-axis is the radial velocity (in km/h).

Among the results of 30 frames per second, only several frames of experiment results are presented with different colors and marks in each frame. Moreover, the measurement time stamps are also displayed. In these results, it was found that the vehicle, bicycle, and pedestrian were detected with different velocities in the BSD zone.

Finally, to evaluate whether a moving car with high speed is detected, an experiment was carried out on a long straight road located outside of DGIST in Figure 23. A car was driving with about 70 km/h velocity.

Figure 24 shows the measured detection results of the developed BSD radar. Here, the x-axis is time (in ms), and the y-axis is the range (in meters) and the radial velocity (in km/h). The range and radial velocity are displayed with blue squares marker and red diamond markers, respectively. Here, it was seen that a moving object with high velocity was also detected well.

In the scenarios mentioned so far, we only considered objects approaching the radar. Vehicles driving in the opposite direction may produce false alarms; however, we can easily determine the moving direction of the object using the sign of the measured velocity.

Moreover, because we only focus on the detection of an object occupying the BSD zone in this paper, the warning decision is beyond the scope of this paper. That is, based on the measured range and velocity, the warning function of the subject car should determine whether it is necessary to provide the driver with a warning.

7. CONCLUSION

In this paper, we designed and developed a 24 GHz automotive blind-spot radar with a low complexity detection

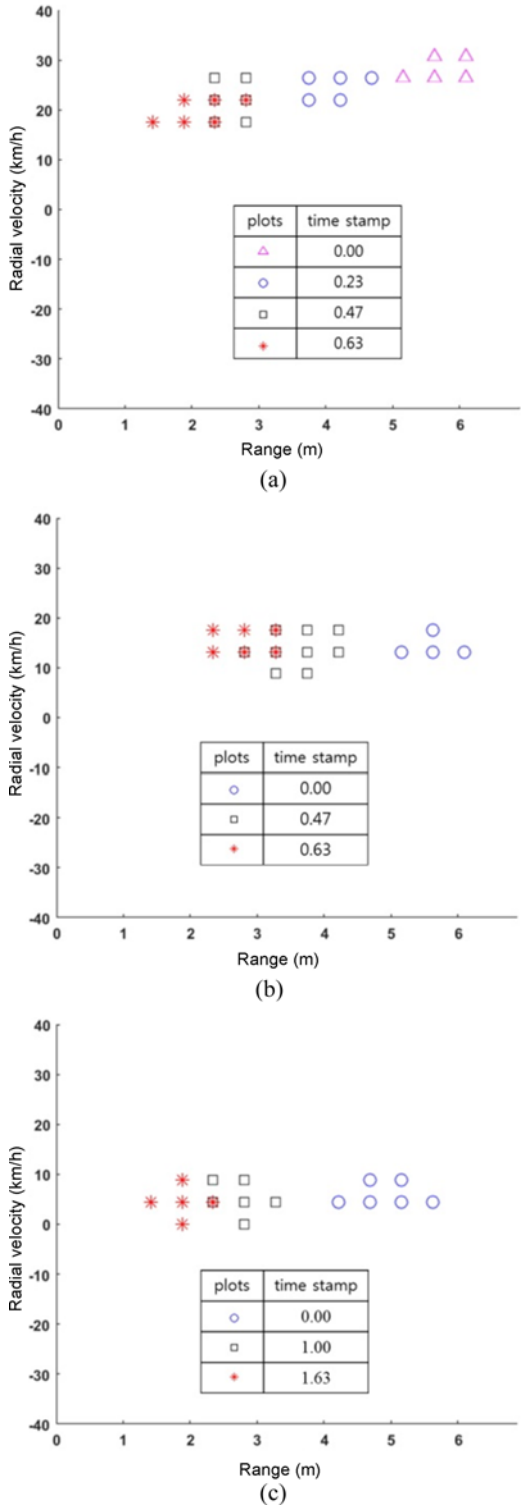

Figure 22. Detection results of three types of targets on an urban road: (a) Car; (b) Bicycle; (c) Pedestrian.

scheme. While the general 2D FFT based detection method is processed using all 2D range-Doppler cells, in the developed radar system, the range and Doppler ROI

Figure 23. Camera views on a long straight road: When entering the detection area (left), and passing through the BSD zone (right).

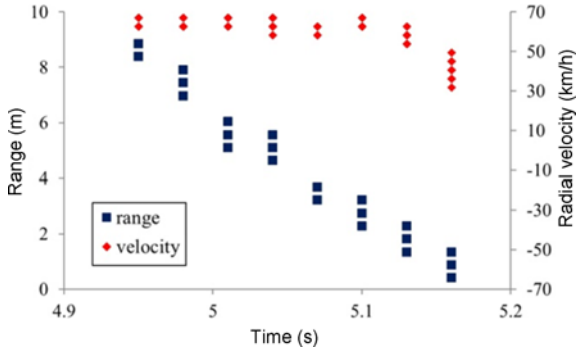

Figure 24. Measured detection results of a high speed car on a straight road: Range (square) and velocity (diamond).

selection are pre-processed before Doppler-processing and CA-CFAR detection, respectively. That is, the Doppler-processing and CA-CFAR detection are only carried out for range ROIs with a high probability of target existence. Moreover, the Doppler ROI cells with a high magnitude in the Doppler-spectrum are only applied in the CA-CFAR processing.

The developed target detection processing scheme was implemented in a TI TMS320 micro-processor. We also developed a 24 GHz BSD FMCW radar transceiver and antennas.

According to the experimental results on a real road, the processing time of the developed architecture was reduced by 52.4 % when the number of range ROIs was 16 and the number of Doppler ROIs in one range-bin was 5. Therefore, the developed automotive BSD radar can be useful for vehicle safety systems at competitive prices.

In this paper, we investigated the effect of the radar installation height and the tilt degree on the detection performance in a clear chamber. Moreover, the detection performance in the developed radar system was verified in a multi-target environment in the same chamber. Next, on a real road, the developed BSD radar system was tested to evaluate whether several types of targets including a vehicle, a bicycle, and a pedestrian, were detected or not. And also, a moving car with high speed of more than about 70 km/h was detected well.

In the future, we will carry out experiments to verify the detection performance using a vehicle deployed with the developed BSD radar system under various road

environments such as highways, urban areas, and tunnels in various weather conditions including rain, snow, and fog, as well as at night time.

ACKNOWLEDGEMENT–This work was supported by the DGIST R&D Program of the Ministry of Science, ICT and Technology of Korea (16-RS-01).

REFERENCES

Bassem, R. M. and Atef, Z. E. (2004). *Simulation for Radar Systems Design*. Chapman & Hall/CRC. London, UK.

Fernández, C., Llorca, D. F., Sotelo, M. A., Daza, I. G., Hellín, A. M. and Álvarez, S. (2013). Real-time vision-based blind spot warning system: Experiments with motorcycles in daytime/nighttime conditions. *Int. J. Automotive Technology* **14**, **1**, 113–122.

Forkenbrock, G., Hoover, R. L., Gerdus, E., Van Buskirk, T. R. and Heitz, M. (2014). Blind Spot Monitoring in Light Vehicles – System Performance. Technical Report of NHTSA (National Highway Traffic Safety Administration), U.S. Department of Transportation).

ISO (2008). Intelligent Transport Systems – Lane Change Decision Aid Systems Performance Requirements and Test Procedure. ISO-17387.

Jeong, S., Lee, J., Choi, S., Oh, J. and Lee, K. (2012). Technology analysis and low-cost design of automotive radar for adaptive cruise control system. *Int. J. Automotive Technology* **13**, **7**, 1133–1140.

Lee, M. and Kim, Y. (2010). Design and performance of a 24-GHz switch-antenna array FMCW radar system for automotive applications. *IEEE Trans. Vehicular Technology* **59**, **5**, 2290–2297.

Lin, B., Chan, Y., Fu, L., Hsiao, P., Chuang, L., Huang, S. and Lo, M. (2012). Integrating appearance and edge features for sedan vehicle detection in the blind-spot area. *IEEE Trans. Intelligent Transportation Systems* **13**, **2**, 737–747.

O'Malley, R., Glavin, M. and Jones, E. (2010). Vision-based detection and tracking of vehicles to the rear with perspective correction in low-light conditions. *IET Intelligent Transport Systems* **5**, **1**, 1–10.

Richards, M. (2005). *Fundamentals of Radar Signal Processing*. McGraw-Hill. New York, USA.

Shunji, M. (2004). New algorithm for multiple object detection in FM-CW radar. *SAE Paper No*. 2004-01-0177.

Texas Instruments (2012). C28x Floating Point Unit DSP Library. User's Guide. FPU-DSP-LIB-UG-V131.

Winkler, V. (2007). Range Doppler detection for automotive FMCW radar. *Proc. IEEE European Radar Conf*., 166–169.